Morphology and dynamics of star dunes from numerical modelling

Deguo Zhang[1], Clément Narteau[1]*, Olivier Rozier[1] and Sylvain Courrech du Pont[2]*

Star dunes are giant, pyramid-shaped dunes composed of interlaced arms. These arms are marked by sinuous crests and slip faces of various directions[1,2]. Their radial symmetry and scale suggest that the star dunes form as a result of complex interactions between a multidirectional wind regime and topography[3,4]. However, despite their ubiquity in modern sand seas[5,6], comparatively little is known about their formation and evolution. Here we present a discrete numerical model of star-dune behaviour based on the feedback mechanisms between wind flow and bedform dynamics[7]. Our simulations indicate that the morphology of star dunes results from the combination of individual longitudinal dunes. We find that the arms of the star dunes propagate only under favourable wind regimes. In contrast to dunes that form from an erodible bed[8], the crests of the propagating arms are oriented such that sand flux is maximized in the direction of arm growth. Our analysis of the simulated three-dimensional structures suggests that the morphodynamics of the arms are controlled by the frequency of wind reorientation, with a high frequency of reorientation leading to smaller arm dimension and high rates of growth. We suggest that arm propagation is an important process of mass exchange in dune fields.

Above a threshold wind velocity at which sand grains start to move, aeolian dunes constantly adapt their shapes in response to the flow[9,10]. In arid deserts on Earth, this permanent reorganization process may lead to the formation of star-dune fields, a regular network of majestic sand hills characterized by a complex tangle of bedforms (Fig. 1a–d). Star-dune-like morphologies may result from amalgamation, the merging of two or more dunes into a single one, or from the development of new arms on a well-established dune pattern[5,11]. In both cases, the role of wind directional variability and secondary flow has been emphasized but not precisely quantified[3]. Moreover, star dunes are the largest aeolian dune pattern in Earth's sand seas[12] so that they integrate wind properties over a wide range of timescales. Then, as for other giant dune types, they exhibit a band-limited hierarchy of superimposed bedforms, from the elementary length scale for the formation of dunes[13,14], $\lambda_{max} \approx 20$ m, to the length scale at which pattern coarsening stops (typically kilometres, the size of star dunes), which is likely to be controlled by the thickness of the convective atmospheric boundary layer[15].

There is still no extensive study on star dunes, essentially because of their size. Up to now, only transient stages of development have been presented using discrete numerical models[16] or underwater laboratory experiments[17]. Nonetheless, the physics of sand dunes under bimodal winds is an active area of research at present.

For the same flow velocity and the same time duration between the two wind reorientations, continuous numerical models[18] and experimental works[19–21] have shown that dunes align longitudinally/transversally to the resultant wind trend if the angle between the wind directions is larger/smaller than 90°. These studies have also suggested that dune morphology (for example, crestline sinuosity, defect density) may be strongly affected by the characteristic time of the bimodal wind. Here, we generalize these observations to multidirectional wind regimes and superimposed bedforms using the output of a real-space cellular automaton model[7,22]. This approach combines a model of sediment transport with a lattice-gas automaton for high Reynolds flow[23] (Fig. 1e–f). This flow is confined in depth so that dune patterns cannot grow indefinitely in height (Methods). We set the length and timescales $\{l_0, t_0\}$ of our discrete numerical scheme to match the conditions met in arid deserts on Earth (Supplementary Information).

Figure 2 shows the formation of star dunes using periodic time functions of wind directionality, with $3 \leq n \leq 7$ regularly spaced wind directions. In all cases, the wind velocity and the mean time t_θ spent in each direction $\theta_i = 2i\pi/n$, $i = \{0, 1, \ldots, n-1\}$ are the same so that the mean flux of sediment is null. Furthermore, sediment leaving the rotating table is reinjected upstream to ensure mass conservation. From an initial truncated conical sand pile, the dune always evolves towards a dynamic equilibrium state that is symmetric with respect to individual wind directions. First, crests develop with trends that maximise the transport perpendicular to their orientation[8] (red insets in Fig. 2). Over longer time periods, whereas there is no arm growth for an even number of wind directions, star-dune arms grow for odd numbers of wind directions. They are then propagating against individual wind directions (blue insets in Fig. 2). This specific arm orientation is robust and resilient to details of time functions of wind directionality and initial conditions. For example, starting from a flat sand bed, dunes first form and grow in height by the primary instability, then merge by pattern coarsening with an organization that reflects the symmetry of the wind regime (Supplementary Information). Once again, the final (giant) dune exhibits arms pointing against individual wind directions (Fig. 1f).

In all simulations, the alignment of the radiating star-dune arms does not maximize the transport perpendicular to the crests as usually expected for longitudinal and transverse dunes[8,20]. Indeed, star-dune arms grow by the transport of sediment over a non-erodible ground, as opposed to the development of bedforms on an erodible sand bed. Naturally, direct measurement of the resultant sediment flux reveals that, during arm growth in zones
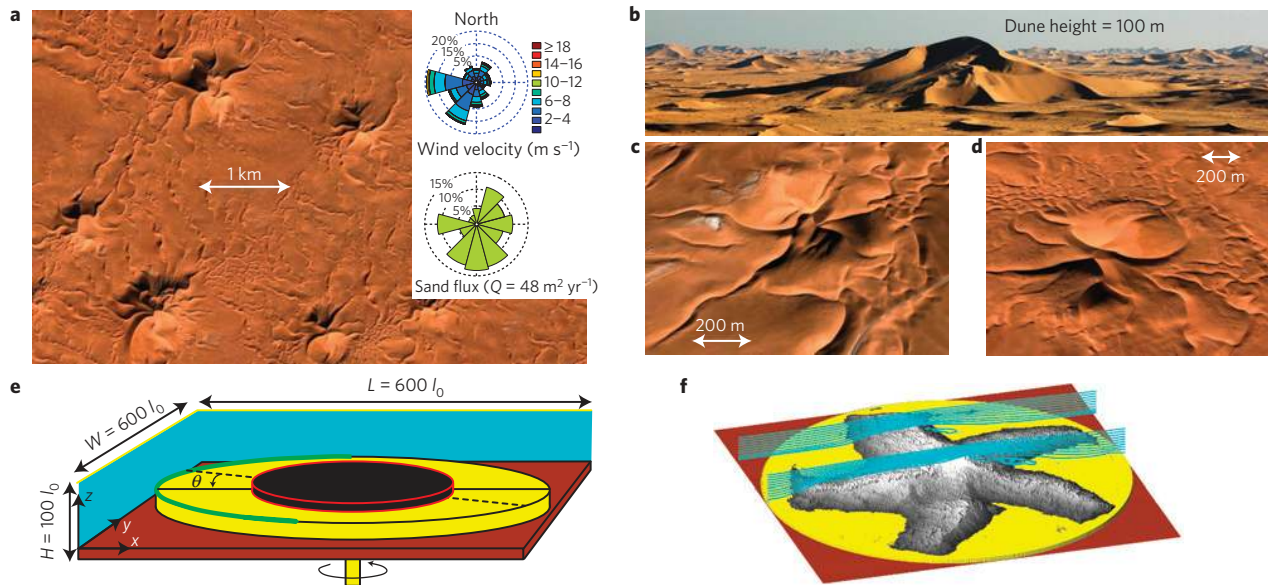
Figure 1 | Star dunes using a real-space cellular automaton model. a, A portion of the Grand Erg Oriental (Algeria, 30° 51′ 53.06″ N, 7° 53′ 52.20″ E). Wind and sand roses are calculated from the Hassi-Messaoud airport data from 2005 to 2009. **b–d**, Lateral and top views of individual star dunes. **e**, A circular rotating table surrounded by removal cells with a semicircle of injection cells upstream is used to reproduce multidirectional wind regimes. *L, W, H* are the length, width and height of the cubic lattice, respectively. **f**, Velocity streamlines above a five-armed star dune using the real-space cellular automaton model (Methods and Supplementary Information).
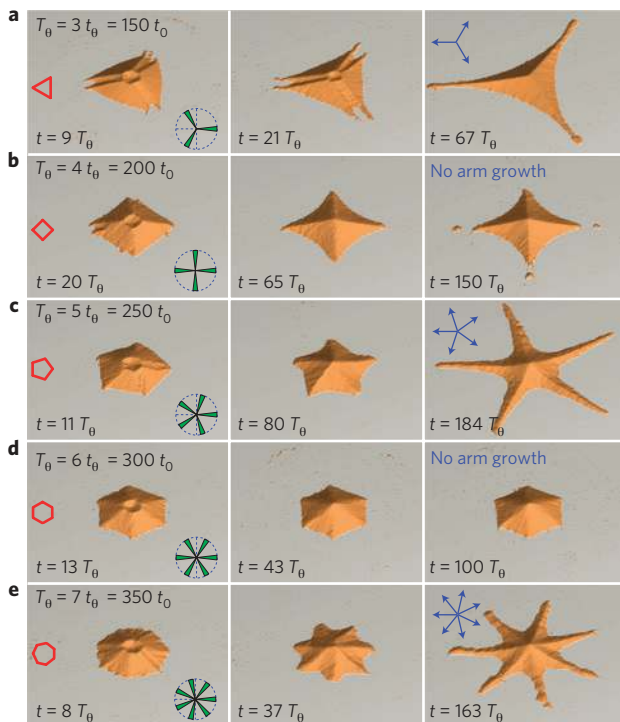

Figure 2 | Formation and evolution of star dunes using multidirectional wind regimes. a–e, From **a** to **e** the wind blows from $n = \{3, 4, \ldots, 7\}$ regularly spaced wind directions $\theta_i = 2\pi i/n$, $i \in \{0, 1, \ldots, n-1\}$, as shown by the wind roses (green insets). The wind speed as the angle and the time delay $t_\theta = T_\theta/n = 50t_0$ between two wind reorientations are constant. Over short timescales, bedform alignment maximizes sediment transport perpendicular to the crest (red insets). Over longer timescales, there is no arm growth for an even number of wind directions. For an odd number, star-dune arms radiate against individual wind directions. Blue insets show the growth direction predicted by equation (1) (Supplementary Information).

of low sediment availability, there is a net flux oriented towards the arm tip, as is the case for isolated longitudinal dunes[20] (Supplementary Information). This growth mechanism imposes that arm alignment maximizes the flux in the direction of arm propagation.

We take advantage of our idealized periodic functions of wind directionality to derive analytical solutions. Let us consider an arm making an angle $\alpha - 2i\pi/n$ with the *i*th wind direction. At zero order and over a complete period $T_\theta = nt_\theta$, the average sand flux in the direction of arm growth writes: $Q_\parallel^0 = (1/T_\theta)\sum_{i=0}^{n-1} Q_0\cos(\alpha - 2i\pi/n)t_\theta$, where Q_0 is the constant sediment flux associated with individual winds. Given our symmetric wind regime with a null resultant wind, $Q_\parallel^0$ is always equal to 0. Hence, the effect of the apparent dune aspect ratio, that is, the dune slope experienced by the wind, on flow velocity and sediment transport has to be taken into account. Including this effect to the first order, the average sand flux writes:

$$Q_\parallel = \frac{1}{T_\theta}\sum_{i=0}^{n-1}\left(Q_0 + Q_1\left|\sin\left(\alpha - \frac{2i\pi}{n}\right)\right|\right)\cos\left(\alpha - \frac{2i\pi}{n}\right)t_\theta \quad (1)$$

where $Q_1 > 0$ is a constant sediment flux associated with a specific aspect ratio, which is assumed to be constant over T_θ. The absolute value term accounts for changes of the apparent dune aspect ratio as seen by individual winds. In agreement with our numerical simulations (Fig. 2), equation (1) predicts that arms radiate against individual winds for odd numbers of wind directions ($Q_\parallel$ is maximum when $\alpha_i = \pi/n + 2i\pi/n$) and no arm growth ($Q_\parallel = 0$ for any α) for even numbers of wind directions. In both cases, the co-existence of crests with different orientations is a consequence of the stability of isolated longitudinal dunes with respect to the wind regime.

To investigate the origin and the orientation of arm growth, we study over long timescales the morphodynamics of a five-armed star dune using a periodic time function of wind directionality with period $T_\theta = 5t_\theta = 300t_0$ (Fig. 3a). Figure 3b maps crestlines during the formation and growth of incipient arms whereas Fig. 3c shows their orientation α_i as a function of their length. Over a short period of time, the sand pile is shaped by the winds and the
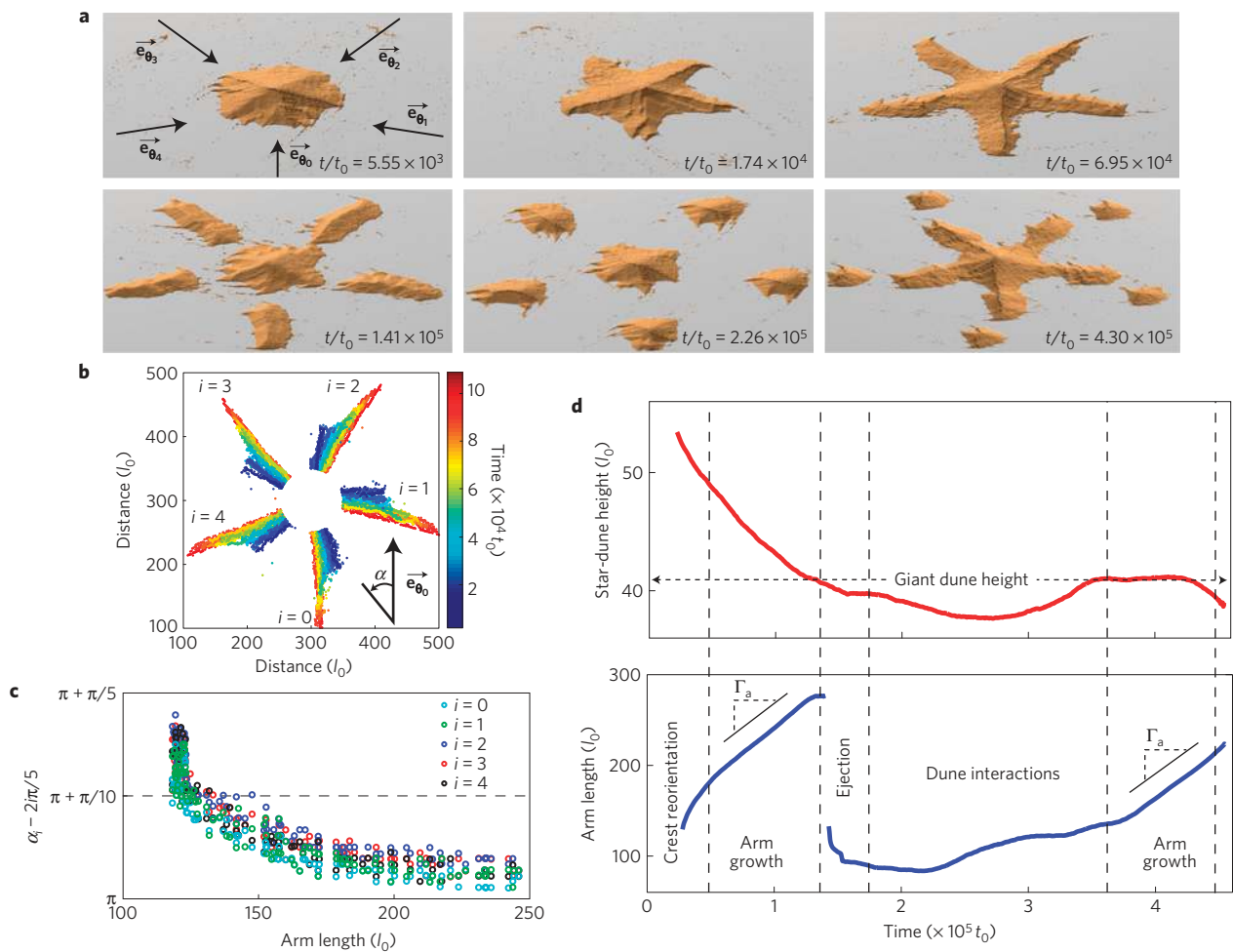
Figure 3 | Star-dune morphodynamics. a, Formation and evolution of a five-armed star dune using $T_\theta = 5t_\theta = 300t_0$ and $\theta = 2\pi/5$. **b**, Crestlines with respect to time. **c**, Direction α_i, $i = \{0, 1, 2, 3, 4\}$ of star-dune arms with respect to their length. Crest reorientation process follows from arm propagation. The $\alpha_i - 2i\pi/5$ value predicted by equation (1) for radiating arms is π. The value $\pi + \pi/10$ (dotted line) corresponds to the trend that would maximize the transport perpendicular to the crest. **d**, Star-dune height and arm length with respect to time. Arms propagate at a constant rate Γ_a when the central dune is giant (or bigger).

alignment rapidly converges to the one that maximizes sediment transport perpendicular to the crest[8], that is, $\alpha_i = \pi/10 + 2i\pi/5$. As the arms start to grow, crestlines operate a global reorientation that maximizes sediment transport in the direction of the radiating arms, that is, $\alpha_i = \pi/5 + 2i\pi/5$ as predicted by equation (1). This arm growth takes sediment from the pyramidal base, which decreases in height. At some point, it becomes too small to feed the arms that eventually detach to create a network of smaller pyramidal dunes interacting with one another. Later, given our specific experimental setup (Fig. 1e), the central dune grows in volume to the detriment of the peripheral dunes. Finally, arms start to radiate again only when the pyramidal dune has reached its maximum height, that is, when it is a giant dune (Fig. 3d,e). Interestingly, the arm growth rate Γ_a is constant regardless of changes between the two periods of arm growth.

Our results, obtained with a model in which the flow is computed in two-dimensional vertical planes, support the idea that there is no need for transverse secondary air flow to give rise to a complex dune shape. Given the stochastic nature of the wind variations (speed, direction), the dynamics of a single star dune in arid sand seas may have additional levels of complexity and transverse secondary air flow may contribute to the final shape of the star dune. Nevertheless, we propose that star dunes are a combination of longitudinal dunes and that their collective behaviours are remotely controlled

by the arm-development mechanism. It is known to be the case in barchan dune corridors where collisions and mass exchange between barchans control their size and alignment[24,25]. Hence, we analyse the morphodynamics of star-dune arms using our periodic function of wind directionality and the three-dimensional sedimentary structures[26] produced by the model (Fig. 4a,b). We find that the propagating arms reach a stationary state characterized by constant width, height and growth rate. Arm width and height increase with an increasing T_θ value (Fig. 4c). There is therefore a dynamic equilibrium between arm dimension and the characteristic time of wind directionality.

Figure 4d shows that the arm growth rate is decreasing as a power law with respect to an increasing T_θ value above a characteristic time T_c, which is here slightly longer than the seasonal timescale on Earth ($700t_0 \approx 1.6$ yr).

If the wind periodicity is shorter than this characteristic time, $T_\theta/T_c < 1$, the growth rate tends to a constant value independent of T_θ. For larger T_θ values, $T_\theta/T_c \geq 1$, arms are not only higher and wider, but arm growth is also inhibited by the development of defects and the detachment of smaller barchanoid dunes at the tip. This dependency of dune morphodynamics on T_θ emphasizes that field studies would gain to take into account and document the frequency with which the wind changes direction in addition to the classical ratio between the resultant drift potential and the drift
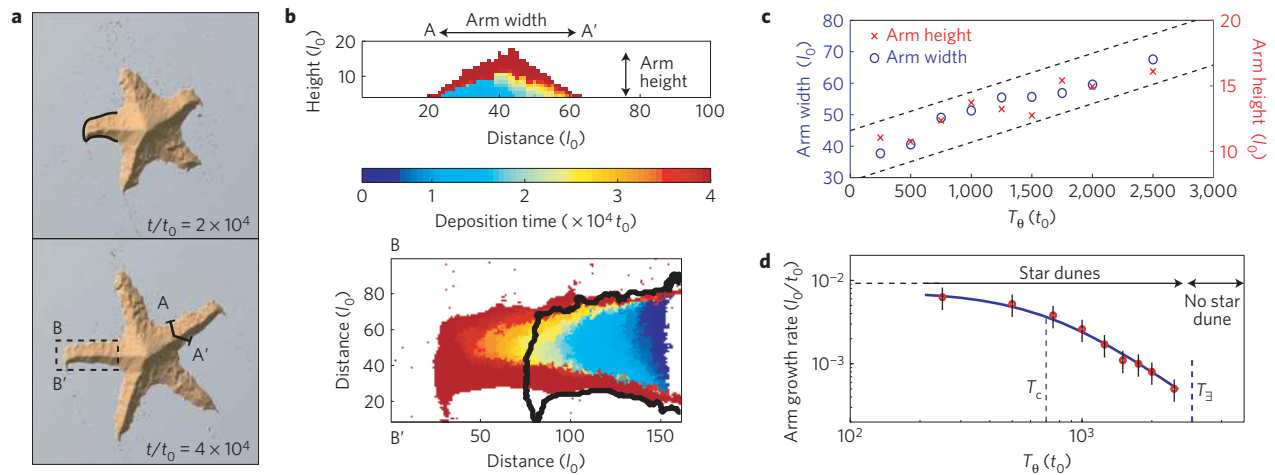
Figure 4 | Effect of the frequency of wind reorientation on arm growth. a, Star-dune development from a conical sand pile using $T_\theta = 5t_\theta = 10^3 t_0$. **b**, Sedimentary structures in a vertical section perpendicular to the crest (top) and a horizontal one just above ground level (bottom). The earlier contour of the arm shows that it grows with a constant width. **c**, Width and height of star-dune arms with respect to T_θ. **d**, Arm growth rate Γ_a with respect to T_θ. As for dashed lines in **c**, error bars are estimated by the standard deviation for the five arms. The solid line is the best fit using $\Gamma_a = A/(1 + (T_\theta/T_c)^2)$, where $A = 7.3 \times 10^{-3} l_0/t_0$ is the maximum growth rate and $T_c = 700t_0$ is the characteristic time above which arm growth is inhibited by ejection of sediment at the arm tip. $T_\exists$ is a critical threshold for the formation of star dunes (Supplementary Information).

potential. Finally, when the T_θ value is larger than a critical timescale $T_\exists$, star dunes cannot form. Instead, the dune shape has time to adapt to individual winds and does not integrate the multimodal nature of the wind regime. As expected, $T_\exists$ decreases with the dune size and transient barchanoid shapes may be observed. Then, assuming that there is a maximum dune size[15], a small wind-direction variability (that is, a large T_θ value and/or large drift potential for individual winds) can prevent the co-existence of dune patterns with different orientations and therefore the appearance of star dunes.

Although dunes are ubiquitous over Mars, there is no star-dune field and the rare incipient three-armed star dunes that have been reported significantly differ from their terrestrial analogues[27]. Furthermore, giant dunes on Mars are expected to be approximately the same size as those on Earth[15,28] for a seasonal timescale that is twice as long (≈ 2 yr). This small wind variability (that is, large T_θ value), together with a relatively small maximum size for dunes is likely to prevent arm growth and the formation of fully developed star dunes on Mars. Such a conclusion is supported by the degree of resemblance between other dune types on Mars and on Earth[29,30] and the omnipresence of martian (mega-)barchans.

Although the simulation of complex dunes would gain from a more detailed airflow modelling including three-dimensional recirculation, we have shown that star dunes may form from primary winds as a superposition of longitudinal dunes. Their morphodynamics depend on the frequency of wind reorientation and crestlines may have two different modes of orientation depending on sand availability. In practice, looking at a pattern, one has to ask if the bedform results from the growth of a wave on a sand bed or from the propagation of an isolated longitudinal dune over a non-erodible ground.

Methods

The real-space cellular automaton model is a hybrid approach[7,22] that combines a model of sediment transport with a lattice-gas cellular automaton for turbulent fluid flow simulation[23] (see Supplementary Information). The model simulates two-dimensional flows in vertical planes aligned with the wind direction and confined by two horizontal walls. We impose no-slip boundary conditions on the bed surface and free-slip boundary conditions along the ceiling as a first approximation of a free surface. By averaging the motion of fluid particles over space and time, we compute the wind velocity (Fig. 1f) and quantify the bed shear stress on the topography. Local erosion rates are then assumed to be linearly related to the shear stress. The sediment in motion reduces the wind velocity at the surface

of the bed; consequently, there is a complete feedback mechanism between the flow and the bedform dynamics.

To set the length and timescales of the real-space cellular automaton model, we use a λ_{max} value of 20 m and estimates of the saturated flux of sediment on a flat sand bed derived from meteorological data file (see wind roses in Fig. 1a and Supplementary Information). Moreover, because of the imposed top boundary condition, dune patterns have a maximum height that scales with the depth H of the fluid layer[22]. Hence, the model reproduces complex structures with a pertinent and controlled range of superimposed bedforms, including giant dunes in Earth's sand seas. In all the simulations presented here, we have $l_0 = 0.5$ m, $t_0 = 2.3 \times 10^{-3}$ yr and a flow depth $H = 100l_0$. To vary wind direction, the simulated dunefield is on a rotating table with a radius of $600\ l_0$ (Fig. 1e).

References

1. Wasson, R. & Hyde, R. Factors determining desert dune type. *Nature* **304**, 337–339 (1983).
2. Lancaster, N. Star dunes. *Prog. Phys. Geogr.* **13**, 67–91 (1989).
3. Lancaster, N. The dynamics of star dunes: An example from the Gran Desertio, Mexico. *Sedimentology* **36**, 273–289 (1989).
4. Zhang, W., Qu, J., Dong, Z., Li, X. & Wang, W. The air flow field and dynamic processes of pyramid dunes. *J. Arid Environ.* **45**, 357–368 (2000).
5. Nielson, J. & Kocurek, G. Surface processes, deposits, and development of star dunes: Dumont dune field, California. *Geol. Soc. Am. Bull.* **99**, 177–186 (1987).
6. Lancaster, N. *Geomorphology of Desert Dunes* (Routledge, 1995).
7. Narteau, C., Zhang, D., Rozier, & Claudin, P. Setting the length and time scales of a cellular automaton dune model from the analysis of superimposed bed forms. *J. Geophys. Res.* **114**, F03006 (2009).
8. Rubin, D. & Hunter, R. Bedform alignment in directionally varying flows. *Science* **237**, 276–278 (1987).
9. Bagnold, R. A. *The Physics of Blown Sand and Desert Dunes* (Methuen, 1941).
10. Pye, K. & Tsoar, H. *Aeolian Sand and Sand Dunes* (Unwin Hyman, 1990).
11. Lancaster, N. in *Eolian Sediments and Processes* (eds Brookfield, M. E. & Ahlbrandt, T. S.) 261–289 (Elsevier, 1983).
12. Breed, C. & Grow, T. in *A Study of Global Sand Seas* (ed. McKee, E.) 252–302 (Professional Paper 1052, US Geological Survey, 1979).
13. Hersen, P., Douady, S. & Andreotti, B. Relevant length scale of barchan dunes. *Phys. Rev. Lett.* **89**, 264301 (2002).
14. Elbelrhiti, H., Claudin, P. & Andreotti, B. Field evidence for surface-wave-induced instability of sand dunes. *Nature* **437**, 720–723 (2005).
15. Andreotti, B., Fourrière, A., Ould-Kaddour, F., Murray, B. & Claudin, P. Size of giant dunes limited by the depth of the atmospheric boundary layer. *Nature* **457**, 1120–1123 (2009).
16. Werner, B. T. Eolian dunes: Computer simulations and attractor interpretation. *Geology* **23**, 1107–1111 (1995).
17. Hersen, P. Flow effects on the morphology and dynamics of aeolian and subaqueous barchan dunes. *J. Geophys. Res.* **110**, F04S07 (2005).

18. Parteli, E. J. R., Durán, O., Tsoar, H., Schwämmle, V. & Herrmann, H. J. Dune formation under bimodal winds. *Proc. Natl Acad. Sci. USA* **106,** 22085–22089 (2009).

19. Rubin, D. & Ikeda, H. Flume experiments on the alignment of transverse, oblique, and longitudinal dunes in directionally varying flows. *Sedimentology* **37,** 673–684 (1990).

20. Reffet, E., Courrech du Pont, S., Hersen, P. & Douady, S. Formation and stability of transverse and longitudinal sand dunes. *Geology* **38,** 491–494 (2010).

21. Taniguchi, K., Endo, N. & Sekiguchi, H. in *EGU General Assembly Conference Abstracts* Vol. 11 (eds Arabelos, D. N. & Tscherning, C. C.) abstr. 6531 (2009).

22. Zhang, D., Narteau, C. & Rozier, O. Morphodynamics of barchan and transverse dunes using a cellular automaton model. *J. Geophys. Res.* **115,** F03041 (2010).

23. Frisch, U., Hasslacher, B. & Pomeau, Y. Lattice-gas automata for the Navier-Stokes equation. *Phys. Rev. Lett.* **56,** 1505–1508 (1986).

24. Cooke, R., Warren, A. & Goudie, A. *Desert Geomorphology* (UCL Press, 1993).

25. Hersen, P. *et al.* Corridors of barchan dunes: Stability and size selection. *Phys. Rev. E* **69,** 011304 (2004).

26. Bristow, C. S., Bailey, S. D. & Lancaster, N. The sedimentary structure of linear sand dunes. *Nature* **406,** 56–59 (2000).

27. Edgett, K. S. & Blumberg, D. G. Star and linear dunes on mars. *Icarus* **112,** 448–464 (1994).

28. Claudin, P. & Andreotti, B. A scaling law for aeolian dunes on Mars, Venus, Earth, and for subaqueous ripples. *Earth Planet Sci. Lett.* **252,** 30–44 (2006).

29. Breed, C., Grolier, M. & McCauley, J. Morphology and distribution of common sand dunes on Mars: Comparison with the Earth. *J. Geophys. Res.* **84,** 8183–8204 (2006).

30. Bourke, M. C. Barchan dune asymmetry: Observations from Mars and Earth. *Icarus* **205,** 183–197 (2010).

Acknowledgements

Author contributions

D.Z. carried out all numerical simulations and statistical data analysis. O.R. developed the real-space cellular automaton, a free sofware under GNU general public license. C.N. and S.C.d.P. designed the study and wrote the manuscript. All authors discussed the results.

Additional information